



UNIVERSITY OF LEEDS

This is a repository copy of *T cell and reticular network co-dependence in HIV infection*.

White Rose Research Online URL for this paper:

<http://eprints.whiterose.ac.uk/94739/>

Version: Accepted Version

Article:

Donavan, GM and Lythe, GD (2016) T cell and reticular network co-dependence in HIV infection. *Journal of Theoretical Biology*, 395. pp. 211-220. ISSN 1095-8541

<https://doi.org/10.1016/j.jtbi.2016.01.040>

© 2016. This manuscript version is made available under the CC-BY-NC-ND 4.0 license
<http://creativecommons.org/licenses/by-nc-nd/4.0/>

Reuse

Unless indicated otherwise, fulltext items are protected by copyright with all rights reserved. The copyright exception in section 29 of the Copyright, Designs and Patents Act 1988 allows the making of a single copy solely for the purpose of non-commercial research or private study within the limits of fair dealing. The publisher or other rights-holder may allow further reproduction and re-use of this version - refer to the White Rose Research Online record for this item. Where records identify the publisher as the copyright holder, users can verify any specific terms of use on the publisher's website.

Takedown

If you consider content in White Rose Research Online to be in breach of UK law, please notify us by emailing eprints@whiterose.ac.uk including the URL of the record and the reason for the withdrawal request.



eprints@whiterose.ac.uk
<https://eprints.whiterose.ac.uk/>

T cell and reticular network co-dependence in HIV infection

Graham M. Donovan^{*†} and Grant Lythe[‡]

4th February 2016

Abstract

Fibroblastic reticular cells (FRC) are arranged on a network in the T cell zone of lymph nodes, forming a scaffold for T cell migration, and providing survival factors, especially interleukin-7 (IL-7). Conversely, CD4⁺ T cells are the major producers of lymphotoxin- β (LT- β), necessary for the construction and maintenance of the FRC network. This interdependence creates the possibility of a vicious cycle, perpetuating loss of both FRC and T cells. Furthermore, evidence that HIV infection is responsible for collagenation of the network suggests that long term loss of network function might be responsible for the attenuated recovery in T cell count seen in HIV patients undergoing antiretroviral therapy (ART). We present computational and mathematical models of this interaction mechanism and subsequent naive CD4⁺ T-cell depletion in which (1) collagen deposition impedes access of naive T cells to IL-7 on the FRC and loss of IL-7 production by loss of FRC network itself, leading to the depletion of naive T cells through increased apoptosis; and (2) depletion of naive T cells as the source of LT- β on which the FRC depend for survival, leads to loss of the network, thereby amplifying and perpetuating the cycle of depletion of both naive T cells and stromal cells. Our computational model explicitly includes an FRC network and its cytokine exchange with a heterogeneous T-cell population. We also derive lumped models, in terms of partial differential equations and reduced to ordinary differential equations, that provide additional insight into the mechanisms at work. The central conclusions are that 1) damage to the reticular network, caused by HIV infection, is a plausible mechanism for attenuated recovery post-ART; 2) within this, the production of T cell survival factors by FRCs may be the key rate-limiting step; and 3) the methods of model reduction and analysis presented are useful for both immunological studies and other contexts in which agent-based models are severely limited by computational cost.

1 Introduction

Our bodies maintain populations of T cells, ready to protect us against invading infections [1]. The survival of T cells relies on the cytokine interleukin-7 (IL-7), that binds to IL-7 receptors on cell surfaces [2–8]. The task of recognition of pathogens and activation of the adaptive immune response is carried out by the T-cell receptor, whose ligands are peptides, associated with major histocompatibility complex (MHC) molecules, on the surface of antigen-presenting cells. The T-cell zones of lymph nodes (LN), where the encounters between T cells and antigen-presenting cells that initiate immune responses occur [9, 10], is also the site where T-cells access the IL-7 resource they need to survive in the absence of infection. One subset of lymph node stromal cells, the fibroblastic reticular cells in the T-cell zone, produce IL-7 [11–16]. Within a T-cell population, IL-7 receptor expression varies from cell to cell; those with higher expression are believed to be more likely to divide [17, 18]. There appear to be altruistic mechanisms at work in CD4⁺ and CD8⁺ T-cell populations: by downregulating IL-7 receptor

^{*}Department of Mathematics, University of Auckland, Private Bag 92019, Auckland, New Zealand

[†]Correspondance: g.donovan@auckland.ac.nz

[‡]Department of Mathematics, University of Leeds, LS29JT, UK

expression in response to IL-7, T cells that have already received survival signals do not outcompete unsignalled T cells for remaining IL-7 [2, 17].

The reticular network (RN) in the T-cell zones of lymph nodes is a system of collagen fibres and extra-cellular matrix wrapped by FRCs [19–22] that provides a scaffold for entry and movement of T cells and for their encounters with dendritic cells [14, 23–25], and a conduit for soluble antigen [26]. The type of random motion exhibited by T-cells [27–31], and two-photon imaging observations when both T cells and stromal cells are visible, are consistent with the idea that T cells crawl along the network, changing direction when they arrive at a vertex connecting edges of the network [32]. FRCs secrete IL-7 and, in return, transiting T cells supply the FRCs of the RN with lymphotoxin- β (LT- β). HIV infection [33–36] disrupts this homeostasis in two ways: 1) increased death rate of T cells (direct killing), and 2) damage to the RN via collagenation, which disrupts cytokine exchange.

Loss of the RN in lymphoid tissues during HIV-1 infection has been shown to impair the survival of naive T cells and limit immune reconstitution after antiretroviral therapy [37, 38]. CD4⁺ T-cell depletion resulted in FRC loss in primates, caused by decreased LT- β mainly produced by the CD4⁺ T cells [39, 40]. These findings led to a hypothesis in which loss of T cell-derived LT- β during HIV-1 infection would lead to loss of RN, which in turn would deplete primarily naive T cells: a vicious cycle perpetuating loss of both FRCs and T cells. The vicious cycle is “closed” because the loss of naive CD4⁺ T cells through collagen-denied access to IL-7 would be the cause of the loss of lymphotoxin and the FRC network that compounds and perpetuates the loss of primarily naive CD4⁺ T cells [39].

Here we develop and analyze models of these cell populations and their interaction via cytokine exchange to explore the plausibility of the experimental hypothesis. Our models are based on the central hypothesis that T cells and FRCs of the RN are mutually dependent via the exchange of cytokines. We simplify by only considering the exchange of IL-7 and LT- β , although other molecules have roles to play, and by considering only one representative lymph node, although there are many. Our cell-based computational model explicitly includes heterogeneity within cell populations, assigning an IL-7 level to each cell. When in the lymph node, each T cell moves along the RN that is made up of FRCs. We use our models to explore the hypothesis that RN collagenation, due to HIV infection, is responsible for the attenuated recovery of T cell counts in HIV patients given (advanced) antiretroviral therapy ((A)ART); that is, the observed partial recovery reflects the loss of overall system capacity due to collagenation or loss of the RN, which is either permanent, or recovers on a longer timescale.

We devise a cell-level representation of T cells, FRCs, and their interactions, based on the experimental hypotheses laid out in the introduction. We use a T cell movement model in which the network is explicitly constructed and individual cells move on it, first developed in [41] and shown to be compatible with existing *in vivo* movement data. The main features of the model are

- IL-7 secretion by FRCs, and collection by migrating T cells
- LT- β secretion by T cells, and deposition onto FRCs
- T cell trafficking between the LN and a bulk periphery
- T cell apoptosis and reproduction (IL-7 dependent)
- FRC apoptosis (LT- β dependent)
- Collagenation of the RN in HIV-infected individuals.
- Direct killing of T cells in HIV-infected individuals.

The combination of large numbers of cells, and long timescales of interest, mean that solutions of the agent-based model are computationally intensive. To address this, we derive a partial differential equation (PDE) population model, retaining the role of distributions of cytokine levels, but neglecting explicit spatial effects of movement on the network. We also consider stochastic models for each population in isolation, equivalent to de-coupling the PDE model, and derive explicit solutions for the steady-state distribution of cell populations. These can further be reduced to a system of ordinary differential equations by assuming steady-state distributions of cytokines.

By examining these reduced models, we can address a number of interesting questions: how is a population of cells maintained? What is the total number of cells, and distribution of expression levels? We devise some simple, stochastic, cell-based rules that are sufficient. By analyzing these models we show that the hypothesis of mutual CD4⁺/FRC population loss in HIV-1 infection is a plausible

mechanism for attenuated recovery after ART, and that the production of the T cell survival factor IL-7 may be the key rate-limiting step in this process. The reduction approach, from an agent-based stochastic model, first averaged into a PDE description which maintains a key role for distribution of cytokine levels, and finally to a set of ODEs applicable near equilibrium, here shows that explicit spatial effects of movement on the RN can be neglected in most situations. The reduction approach is potentially useful in many contexts [42, 43].

2 Model

2.1 T cell circulation

The circulation of T cells through the body is represented by transit between two compartments. A T cell in the first, peripheral, compartment has a probability per unit time, ρ , of transfer to the second, lymph node, compartment. The lymph node compartment, in the model, is a single static network, representing the T-cell zone of a typical lymph node [41]; a T cell enters at a location randomly selected from the “entrance” nodes, and moves along the network until it finds one of the parts of the network that is designated as an exit. Cells migrating on the network collect the IL-7 produced by the FRCs, and conversely deposit LT- β , at rate γ , as they pass. A T cell in the periphery, provided it has accumulated an IL-7 count above the threshold, X , may divide, with probability per unit time λ , in which case the mother cell divides its IL-7 equally between two daughter cells.¹ All T cells, in either spatial compartment, may die, with probability per unit time μ . The circulation model is illustrated schematically in Fig. 1.

The RN is constructed of FRCs of uniform size, aligned in straight edges connected at nodes. As long as they are not collagen-coated, these cells produce IL-7 at a constant rate, ν , that can be picked up by T cells that pass along the edge. A subset of RN edges are “exit” edges, and cells arriving there exit to a bulk periphery. T cells move on the edges of the network with constant speed v . When they arrive at a vertex, they select one of the available edges at random and continue.

Each T cell has an attribute that varies from cell to cell, and depends on time, that we imagine as an IL-7 level and denote by x . Cells with values of x less than X cannot undergo division. A T cell in the periphery, provided it has $x > X$, has probability per unit time, λ , of undergoing division, in which case its IL-7 is divided equally between two daughter cells. Any IL-7 carried by a cell which undergoes apoptosis is lost. Formulated in this way [44], the model is solved via Monte Carlo simulation [45], which is conceptually simple but extremely computationally expensive. Additional details of the model, and some of its properties, are given in Appendix A.

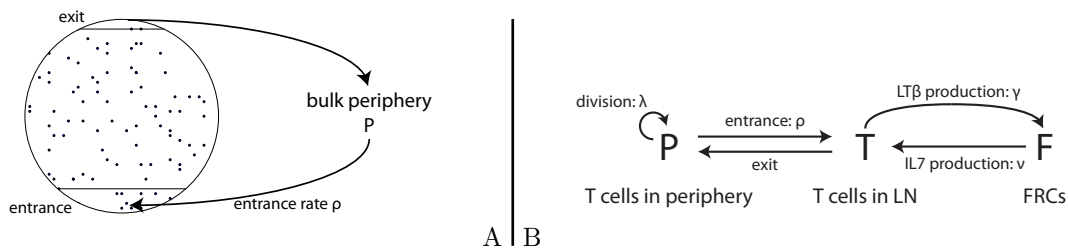


Figure 1: Schematic illustration of the detailed dynamics model. A: Geometry of LN and trafficking to the bulk periphery. B: Interaction mechanisms between the cell populations.

The effect of HIV infection is twofold: 1) direct killing of T cells, and 2) collagenation of the RN (which blocks cytokine exchange between FRCs and T cells). We do not attempt to quantify these

¹Here for simplicity we assume that T cells divide only in the bulk periphery and not while migrating the network. This assumption is easily relaxed, with consequences discussed in Sec. 5.

phenomena with explicit parameters, but instead explore the extent to which such changes can disrupt the cytokine-based symbiosis between T cells and FRCs. In order to do so, we consider several reduced models which allow either analytic solutions or reduced computational complexity.

3 Maintaining a heterogeneous population

As T cells circulate through the lymph node and peripheral compartments of our model, a homeostasis of the heterogeneous T-cell population is established. On the one hand, steady state value of total IL-7 is established by a balance between production by FRC, and consumption by T-cells. On the other hand, a dynamically-maintained stationary distribution of values of x (the IL-7 level) is also established. Each cell has a time-dependent value of x , but the distribution of values in a population of cells may take a form that does not depend on time.

In this section, we investigate the stationary density of values of x over a population of cells, given only the following assumptions:

- The physiological environment provides a constant production rate of IL-7, ν , that is equally likely to be captured by all living cells.
- Each cell has an IL-7 ‘level’, x , that is a function of time. Cells with level above a threshold, X , enter cell division with rate λ .
- When a cell i divides, each daughter cell begins life with IL-7 level $x_i/2$.
- Each cell, independently of all others and of IL-7 level, has a probability μ per unit time (rate) of death.

In order to derive equations governing these processes, we consider the probability density function for the IL-7 level of a T cell as $c(x, t)$, which then gives us

$$\mathcal{P}[\text{randomly-chosen cell has IL-7 level} < x \text{ at time } t] = \int_0^x c(y, t) dy.$$

Further suppose there are $n(t)$ cells at time t . Then in a small time interval Δt , the mean number of cells that die is $\mu n(t)\Delta t$ and the mean number of cells that divide is $\lambda f(t)n(t)\Delta t$, where $f(t)$ is the fraction of cells with IL-7 level above the reproduction threshold X :

$$\int_X^\infty c(x, t) dx = f(t).$$

Thus, a steady-state balance between birth and death of cells requires

$$\lim_{t \rightarrow \infty} f(t) = \frac{\mu}{\lambda}. \quad (1)$$

Let the mean IL-7 level in the steady state be \bar{x} :

$$\bar{x} = \lim_{t \rightarrow \infty} \int_0^\infty x c(x, t) dx.$$

Balance between production of IL-7 (at rate ν) and consumption of IL-7 implies $\mu \bar{n} \bar{x} = \nu$, where $\bar{n} = \lim_{t \rightarrow \infty} \mathbb{E}(n(t))$, or

$$\bar{n} = \frac{\nu}{\mu \bar{x}}. \quad (2)$$

Now consider the changes in a small time interval Δt , as $\Delta t \rightarrow 0$. At most one of three things may happen to a randomly-selected cell. Firstly, it may acquire a unit of IL-7, with probability $\frac{\nu}{n(t)} \Delta t$.

Secondly, it may die with probability $\mu\Delta t$. Thirdly, if the cell's value of x is not less than X , the cell may divide, with probability $\lambda\Delta t$. As a cell with level x divides, it becomes a pair of cells each with $x/2$. Hence, the set of cells with values of x in the interval $[2x, 2x + 2\Delta x]$ divide into a pair of daughter cells which are then in the interval $[x, x + \Delta x]$. Then as $\Delta t \rightarrow 0$, we combine these effects to obtain

$$c(x, t + \Delta t) = \begin{cases} c(x, t)(1 - \mu\Delta t) + 4\lambda c(2x, t)\Delta t + \frac{\nu}{n(t)}(c(x-1, t) - c(x, t))\Delta t & x \leq X, \\ c(x, t)(1 - (\mu + \lambda)\Delta t) + 4\lambda c(2x, t)\Delta t + \frac{\nu}{n(t)}(c(x-1, t) - c(x, t))\Delta t & x > X. \end{cases} \quad (3)$$

With the approximation $c(x-1, t) - c(x, t) = \frac{\partial c}{\partial x}(x, t)$, which is valid if $x \gg 1$, and $[c(x, t + \Delta t) - c(x, t)] / \Delta t = \frac{\partial c}{\partial t}(x, t)$, valid for small Δt , we find

$$\frac{\partial c}{\partial t}(x, t) = \begin{cases} -\mu c(x, t) + 4\lambda c(2x, t) - \frac{\nu}{n(t)} \frac{\partial c}{\partial x}(x, t) & x \leq X, \\ -(\mu + \lambda)c(x, t) + 4\lambda c(2x, t) - \frac{\nu}{n(t)} \frac{\partial c}{\partial x}(x, t) & x > X. \end{cases} \quad (4)$$

Then to derive an expression for the stationary IL-7 density in the heterogeneous population model,

$$C(x) = \lim_{t \rightarrow \infty} c(x, t),$$

we define

$$\alpha = \frac{\bar{x}}{1 + \frac{\lambda}{\mu}} \quad \text{and} \quad \beta = \frac{4\lambda}{\mu + \lambda}.$$

The stationary density satisfies

$$\alpha \frac{dC}{dx} = -C(x) + \beta C(2x) \quad x \geq X$$

and

$$\bar{x} \frac{dC}{dx} = -C(x) + 4 \frac{\lambda}{\mu} C(2x) \quad X/2 < x < X.$$

The solution of these equations is found in Appendix B and plotted in Fig. 2, giving the characteristic shape of the steady-state distribution.

4 PDE population models

The cell-based postulates in Section 3 are a simple way to understand the maintenance of a single, but heterogeneous, cell population, with a distribution of values of the attribute x . In this Section, we develop a PDE representation of the three interacting cell populations of our system: T cells in the periphery, T cells in the LN compartment, and FRC cells. The time-dependent distribution of values of I , the attribute of T cells that describes an accumulation of IL-7 signal, is coupled to that of values of L , attribute of FRCs that describes its accumulation of LT- β .

$T(I, t)$ is the time- and IL-7-dependent distribution of T cells on the network; similarly $P(I, t)$ is the distribution of T cells in the bulk periphery, and $F(L, t)$ is the LT- β dependent distribution of the FRCs forming the RN. Then, based on the model developed in Section 3, we can write

$$\frac{\partial T}{\partial t} = -\mu T - c_o T + \rho P - \bar{\nu} \frac{\bar{F} g(\bar{T})}{\bar{T}} \frac{\partial T}{\partial I} \quad (5a)$$

$$\frac{\partial P}{\partial t} = -\mu P + c_o T - \rho P + \begin{cases} 0, & I < X/2 \\ 4\lambda P(2I, t), & X/2 \leq I \leq X \\ -\lambda P(I, t) + 4\lambda P(2I, t), & I > X \end{cases} \quad (5b)$$

$$\frac{\partial F}{\partial t} = \beta \frac{\partial F}{\partial L} - \gamma \frac{\bar{T}}{\bar{F}} \Big|_{t=0} \frac{\partial F}{\partial L} + \frac{D}{2} \frac{\partial^2 F}{\partial L^2} - \kappa F, \text{ for } L \in [\hat{L}, \infty) \text{ with } F(\hat{L}, 0) = 0. \quad (5c)$$

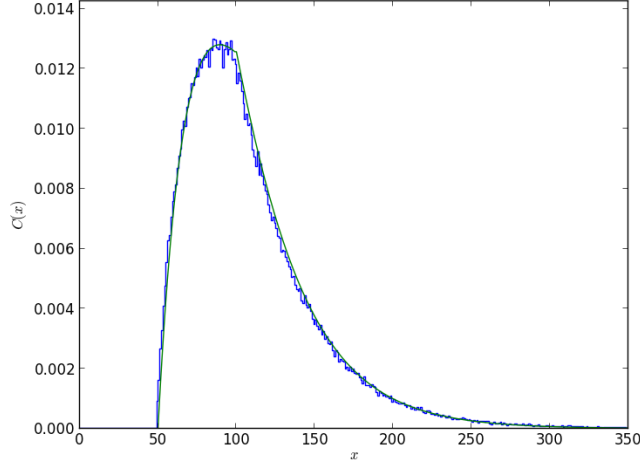


Figure 2: Histogram of values of x in the heterogeneous T-cell population model. The analytical solution (solid line) is compared with direct numerics, with $\mu = 1.0$, $\lambda = 2.0$, $X = 10^2$, $\nu = 4 \times 10^4$.

Here we have defined total cell counts, denoted with the overbar, as

$$\begin{aligned}\bar{T}(t) &= \int_0^\infty T(I, t) dI, \\ \bar{P}(t) &= \int_0^\infty P(I, t) dI, \\ \bar{F}(t) &= \int_{\hat{L}}^\infty F(L, t) dL\end{aligned}$$

and also

$$\begin{aligned}D &= \beta + \gamma \frac{\bar{T}}{\bar{F}|_{t=0}} \quad \text{and} \\ g(\bar{T}) &= 2 \left(\frac{1}{1 + e^{-\bar{T}/\bar{T}_0}} - \frac{1}{2} \right).\end{aligned}$$

The equations for T and P , 5a and 5b, are adaptations of the sharing model, with transiting between the two populations with rates c_0 ($T \rightarrow P$) and ρ ($P \rightarrow T$). The equation for F 5c is a Fokker-Planck approximation of the birth-death process [46], where “birth” and “death” are collection of LT- β and consumption of LT- β , respectively. Consumption of LT- β occurs at a rate per FRC, hence the simple term $\beta \frac{\partial F}{\partial L}$; collection, on the other hand, depends on the production, which occurs per unit of T , but also the collection efficiency. Thus total LT- β production is $\gamma \bar{T}$, but this is distributed over the entire network, and so the LT- β actually collected by an average, active FRC is $\gamma \bar{T} / [\bar{F}|_{t=0}]$. Because FRCs die when their LT- β level falls below \hat{L} we have the homogeneous Dirichlet condition at $L = \hat{L}$. We also include the term $-\kappa F$ in 5c as loss of FRCs due to HIV-induced collagenation.

All parameters are directly equivalent to their counterparts from microscopic dynamics except for c_0 and \bar{T}_0 . The parameter c_0 is easily approximated as $1/\tau$, where τ is the mean network transit time, discussed in Appendix A. The parameter \bar{T}_0 describes the network saturation dynamics. By way of comparison with the model of Sec. 3, here we use $\tilde{\nu} \sim \nu/n$ representing the mean IL-7 collection rate per T cell. Parameter values are discussed fully in Appendix A.

4.1 HIV infection and ART

We first attempt to establish the effects of HIV infection, which can affect the system both by direct killing of T cells, and by collagenation of the RN. Comparison with experimental data allows us to estimate parameters in order to see the relative contributions of each process.

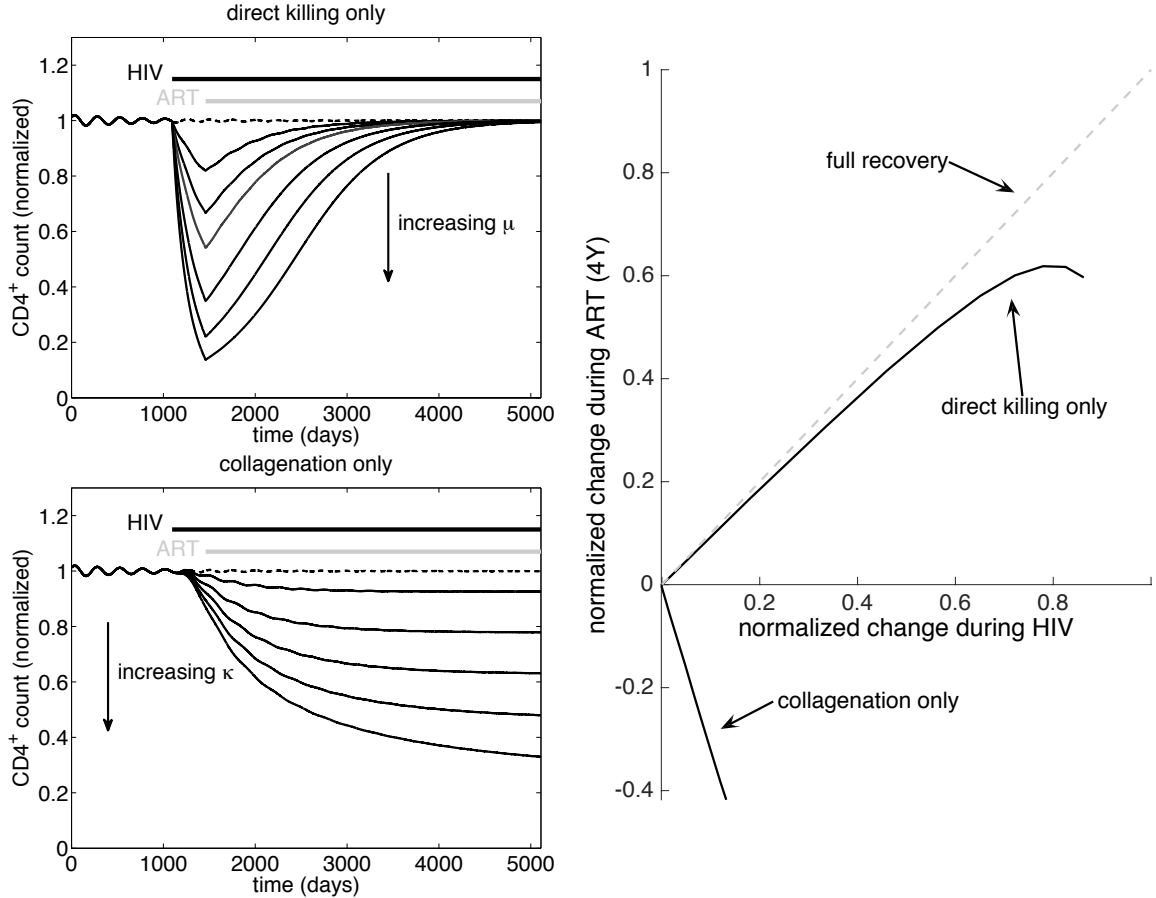


Figure 3: **Response to HIV and ART.** Upper left panel: HIV is simulated with direct killing of T cells only, for a range of values of μ . T cell loss during active HIV is severe, but the recovery during ART is close to full. Lower left panel: simulated collagenation of the RN only, for a range of κ . Here modest T cell loss during HIV is followed by further loss during ART, due to persistent damage to the RN. Right-hand panel: same data, comparing the change in cell count during HIV alone with the change in cell count during ART.

To do so, we begin by applying independent changes to two parameters, one associated with each effect. Increased death of T cells in individuals with HIV infection is implemented via the T cell death rate parameter μ and collagenation of the RN, by the parameter κ . We assume that ART is entirely effective in that both parameter values return to baseline during ART. In Fig. 3 we show the effects of altering each parameter separately. In the upper left panel, HIV is simulated with direct killing of T cells only (no collagenation of the RN, $\kappa = 0$) for a range of values of the direct killing parameter. In this case, while T cell loss during active HIV can be severe, the recovery during ART is close to full. On the other hand, the lower left panel gives the results for simulating collagenation of the RN only (no direct killing), again for a range of values of this parameter. Here the result is quite different: relatively modest T cell loss during the unmitigated HIV phase is paired with further loss during

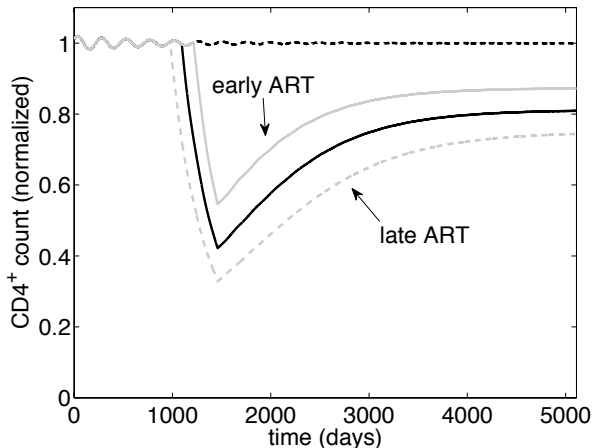


Figure 4: Simulated ART treatment of HIV with different exposure times; parameters for HIV fitted to the data of [47].

ART, due to persistent damage to the RN. The right-hand panel presents the same data in a different manner, comparing the change in cell count during HIV alone with the change in cell count during ART. T-cell counts recover from the effects of direct killing, except in cases of severe depletion, while there is no recovery (and instead further decline) from collagenation.

Given this information on the distinct roles of direct killing and collagenation, it is then possible to estimate the values of these parameters during HIV. Taking the data of [47] to make a first estimate we target an initial reduction of 57% from baseline after 1 year of HIV ($CD4^+$ count declining from ~ 1000 cells/mm³ to ~ 430 cells/mm³) and a subsequent recovery of 31% after 4 years of ART ($CD4^+$ count recovering from ~ 430 cells/mm³ to ~ 740 cells/mm³). Using this calibration we find $\mu_{HIV} = 5.4 \times 10^{-3}/\text{day}$ and $\kappa = 3.8 \times 10^{-4}/\text{day}^2$, and the results of this simulation are given by the solid black curve in Fig. 4. Here we can also easily test the effects of introducing ART relatively earlier or later, as considered by [47], shifting the HIV exposure time by 120 days in each direction; of course greater exposure time without ART results in greater $CD4^+$ count decline during this phase, but also the recovery is altered because of the level of RN damage from collagenation, with changes of ± 120 days resulting in $\pm 6.5\%$ changes in recovery, respectively.

It is worth noting that this is a relatively simplistic treatment, assuming that the only possible roles of HIV in the system are changes to μ and κ . Other possibilities include changes to cell motility, which would alter c_0 and perhaps ρ , but in such an environment more data would be needed in order to determine the parameters.

4.2 Validation of PDE model

To compare solutions between the full model and the PDE approximation, we devise a test problem at the limits of the computational complexity for the former case. Specifically, we construct a network with 5,000 vertices which supports approximately 5,000 T cells at homeostatic equilibrium; we then simulate for 5 years and the results are given in Fig. 5. The qualitative agreement is good given the approximations made; in terms of computational cost, simulating the microscopic dynamics takes ~ 43 hours on a modern workstation, while the PDEs can be solved accurately in less than 8 minutes. Here we compare only distribution of T cells with respect to IL-7, with the histogram in the case of the full

²In terms per year: $\mu_{HIV} = 1.97/\text{year}$ and $\kappa = 0.14/\text{year}$

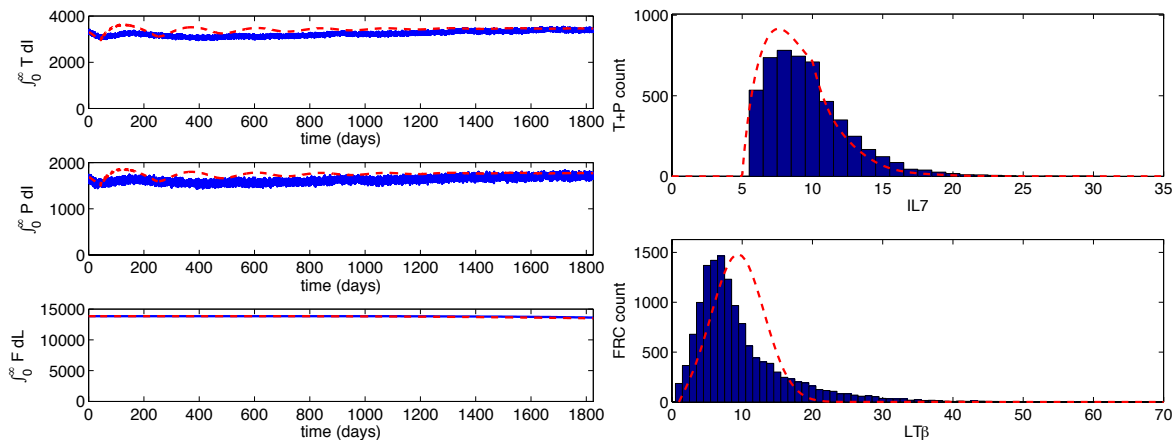


Figure 5: Validation of PDE model against simulation of detailed dynamics; PDE results are red, dashed – full model in blue. Time courses of cell populations are given in the left panels, and comparisons of the final distributions at 5 years in the right panels.

model, and the probability density of the PDE-based model. Given the approximations, the agreement is very good.

4.2.1 Dependence of $CD4^+$ count changes on baseline count and collagenation

For an additional comparison with the limited experimental data which is available, we make model predictions of T cell population change (after 6 months), as a function of both initial T cell population size and the fraction of the RN covered with collagen; the simulation results are given in Fig. 6. This protocol is structured for comparison with that of Schacker et al. [37] so as to make a direct comparison with their Fig. 1, showing that, in both studies, the change in the T cell count is proportional to the baseline count, but inversely proportional to the collagenation fraction. There are several differences worth noting between the predictions of [37] and Fig. 6. First, here we predict relatively smaller changes in T cell count after six months, especially at low collagenation levels.³ Second, the dependence on collagenation level is closer to linear, rather than saturating. And third, as the baseline count approaches the homeostatic equilibrium, the predicted change declines as there is less scope for recovery. Still, the key qualitative aspects, especially inversely proportionality to the collagenation fraction, are clear.

³This is in part a difference of recovery timescale, in that our populations are recovering rapidly after 6 months; if we instead look after 1 year, the comparison improves markedly.

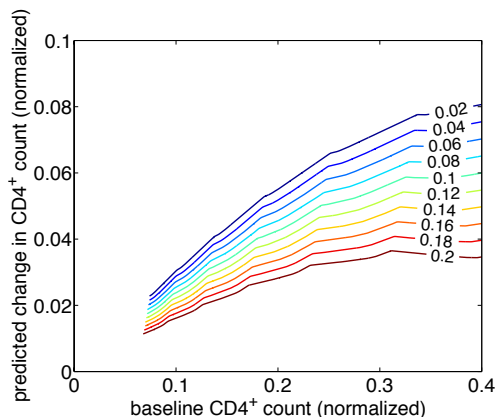


Figure 6: Model predictions of T cell population change after 6 months, as a function of both initial T cell population size (x axis) and the fraction of the RN covered with collagen (labelled in figure). The simulation protocol is designed to mimic Schacker et al. [37] and provide direct comparison with their Fig. 1.

5 Compartments and an ODE approximation

We can reduce the PDE model to an ODE model by integrating with respect to cytokine levels and making assumptions about the equilibrium distributions of cytokine levels, yielding a linearized⁴ compartmental model as follows:

$$\frac{d}{dt}T = \rho P - c_0 T - \mu T - \tilde{\nu} f T \quad (6a)$$

$$\frac{d}{dt}P = c_0 T - \rho P - \mu P + 2\lambda P^* \quad (6b)$$

$$\frac{d}{dt}T^* = \rho P^* + \tilde{\nu} f T - c_0 T^* - \mu T^* \quad (6c)$$

$$\frac{d}{dt}P^* = -\rho P^* - \mu P^* + c_0 T^* - \lambda P^*. \quad (6d)$$

where T and P are the sub-threshold populations (e.g. $I < X$), while the starred versions are super-threshold. A derivation is given in Appendix C. The interactions can be understood schematically as illustrated in the left panel of Fig. 7.

This formulation allows us to understand more readily the role of the parameters. For example, it is easy to show, at equilibrium, that

$$P^* = \frac{\mu}{\lambda}(T + T^* + P + P^*). \quad (7)$$

That is, the fraction of T cells which are available for reproduction (in the bulk periphery, and over threshold) is determined only by the apoptosis parameter μ and the reproduction rate λ . A comparison of this ratio with the full model is given in the right panel of Fig. 7. Other ratios can be similarly

⁴This model is not necessarily appropriate for direct solution as-is, because of the linearization. For example, 6a–6d have only the trivial equilibrium unless the parameters are chosen such that the coefficient matrix has determinant equal to zero. This is because the underlying nonlinearity has been approximated away into the new constant f (see Appendix C); retaining the nonlinearity allows for the nontrivial (homeostatic) equilibrium, but greatly complicates the analysis. However, useful insight about the system behaviour can still be inferred.

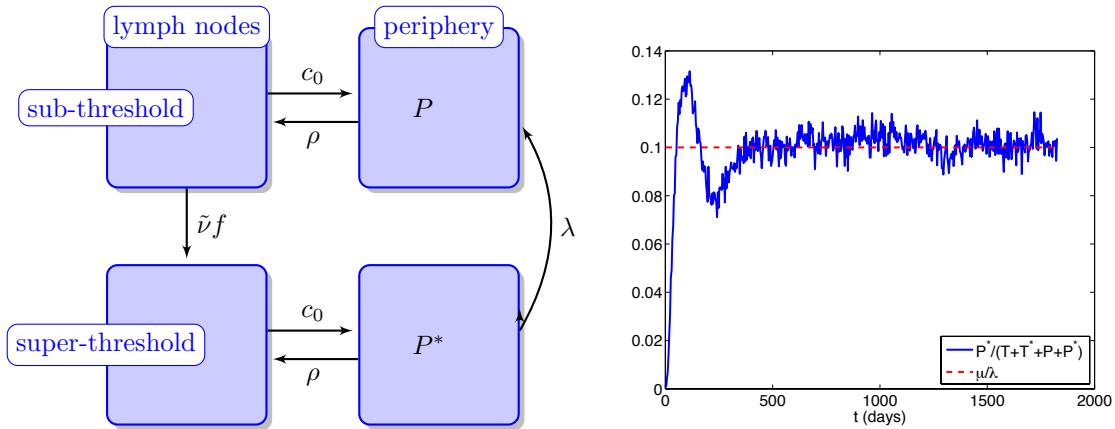


Figure 7: Left panel: compartment model of T-cell homeostasis. Right panel: Comparison of steady state cell population ratios between the compartmental ODE model, and the full computational model.

derived, for example

$$\frac{T}{P} = \frac{\rho}{c_0 + \mu + \tilde{\nu}f}, \text{ and} \quad (8)$$

$$\frac{T^*}{P^*} = \frac{\rho + \mu + \lambda}{c_0}. \quad (9)$$

Equation 7 was selected for direct comparison with the full simulations because it depends only on explicitly-known parameters; however, using approximations to the indirect parameters, the other ratios also have favourable comparisons.

Similarly, suppose we wish to relax the assumption that only peripheral T cells may divide, and instead allow reproduction of T cells in the LN (following the same rules). Thus we must add two terms, $+2\lambda T^*$ to the right hand side of 6a, and $-\lambda T^*$ to the right-hand side of 6c. Then the same type of equilibrium ratios can be derived, for example the equivalent of 7 is now

$$T^* + P^* = \frac{\mu}{\lambda}(T + T^* + P + P^*), \quad (10)$$

that is, the fraction of cells available for reproduction is unchanged.

6 Discussion

In this study we have constructed a sequence of mathematical models based on the experimental hypothesis that FRC and T cell populations are mutually dependent via cytokine exchange and normally establish a homeostatic equilibrium. More specifically, we use this framework to consider the extent to which damage to the RN, in the form of HIV-induced collagen deposition, could be responsible for the characteristic attenuated recovery seen in HIV patients post-ART. We show not only the plausibility of this hypothesis, but explore the more specific mechanisms and dependencies via which it may occur.

In order to do so, we formulate first an explicit (agent-based) model which accounts for movements of individual T cells in relation to the RN. While this model has advantages in terms of explicit inclusion of the movement dynamics, it has drawbacks in terms of the computational cost of simulating it (because of the relatively short timescale of the movement dynamics (e.g. < 1 min), the large number of cells involved, and the relatively long periods of physiological interest (years)). To address these issues, we derive a series of reduced models by averaging the spatial effects.

First we derive a PDE-based model which retains a key role for the distribution of cytokine levels within each cell population. Using this model we are able to explore the means by which HIV disrupts the T cell-FRC homeostatic equilibrium, and the extent to which ART is able to affect a recovery. We show that direct killing of T cells by HIV, even if resulting in significant depletion during the unmitigated HIV phase, is almost entirely reversible by ART. Only when $CD4^+$ depletion reaches roughly 70% from direct killing only does the recovery become attenuated. On the other hand, collagenation of the RN in isolation from direct T cell killing has a relatively modest effect during HIV without ART, but here the changes are persistent and in fact the declines continue even after ART is introduced. Thus using these two factors and a comprehensive set of clinical data, we are able to estimate the relative contributions of both direct killing and RN collagenation in HIV, the subsequent reversal which occurs. We also show that this reversal is dependent on the timing of ART introduction, as in [47], with earlier ART leading to closer to full recovery.

We also show that this PDE-based model agrees well with the agent-based model with explicit spatial dynamics, and also the experimental data of Schacker et al. [37], in terms of the qualitative dependence of T cell population changes on both baseline population levels, and collagenation levels (despite the quantitative differences pointed out in Sec. 4.2.1).

While this PDE-based model has much more modest computational cost, it still must be solved numerically. In order to better understand some of the underlying processes, we derive further reductions under specific assumptions. The first of these is to understand how the population of a single cell type is maintained by the interacting processes of cytokine provision, cell reproduction, and death. This results in the decoupling of the PDE-based model system, and the single PDE remaining can be solved explicitly at steady-state. While derived for the specific biology of this problem, the population maintenance ideas should be applicable in many other similar contexts.

The second reduction retains the interacting cell populations (T cells in the LN, T cells in the periphery, FRCs), but we assume that the distributions of cytokine levels within each population are at steady state; by doing so we can reduce the coupled partial differential equations to coupled ordinary differential equations. These ODEs can then be used to derive key ratios which explain the population behaviours in terms of the underlying parameters, for example that the fraction of cells available for reproduction depends only on the T cell death rate μ and the reproduction rate λ .

Thus the conclusions of this study might be divided into two groups: first, the specific biological implications for the process of T cell-FRC interdependence, its disruption by HIV, and recovery in ART; and second, that the more general process of reducing the agent based model, by degrees, can allow a much more complete understanding of complex biological systems than is possible by examining any one model alone.

As with any model, there are a number of assumptions and limitations which should be noted. In particular, we consider only two signalling agents, $LT-\beta$ and $IL-7$, and the dynamics of the T cells on the network, and the geometry of the network itself, is simplistic. Still, the models as constructed suggest that the interactions between T cell and FRC populations play an important role in maintaining both populations and governing response to both HIV and ART.

References

- [1] K. Takada and S.C. Jameson. Naive T cell homeostasis: from awareness of space to a sense of place. *Nature Reviews Immunology*, 9(12):823–832, 2009.
- [2] Terry J Fry and Crystal L Mackall. The many faces of $IL-7$: from lymphopoiesis to peripheral T cell maintenance. *Journal of Immunology*, 174(11):6571–6576, 2005.
- [3] Benedict Seddon and Rose Zamoyska. Regulation of peripheral T-cell homeostasis by receptor signalling. *Current Opinion in Immunology*, 15(3):321–324, 2003.
- [4] J. Hataye, J.J. Moon, A. Khoruts, C. Reilly, and M.K. Jenkins. Naive and memory $CD4^+$ T cell survival controlled by clonal abundance. *Science*, 312(5770):114, 2006.

- [5] Renata Mazzucchelli and Scott K Durum. Interleukin-7 receptor expression: intelligent design. *Nature Reviews Immunology*, 7(2):144–154, 2007.
- [6] R. Varma. TCR triggering by the pMHC complex: valency, affinity, and dynamics. *Science's STKE*, 1(19):pe21, 2008.
- [7] Joyce T Tan, Eric Dudl, Eric LeRoy, Richard Murray, Jonathan Sprent, Kenneth I Weinberg, and Charles D Surh. IL-7 is critical for homeostatic proliferation and survival of naive T cells. *Proceedings of the National Academy of Sciences*, 98(15):8732–8737, 2001.
- [8] Paul Koenen, Susanne Heinzl, Emma M Carrington, Lina Hoppo, Warren S Alexander, Jian-Guo Zhang, Marco J Herold, Clare L Scott, Andrew M Lew, Andreas Strasser, and Philip D. Hodgkin. Mutually exclusive regulation of T cell survival by IL-7R and antigen receptor-induced signals. *Nature Communications*, 4:1735, 2013.
- [9] P. Bousso and E. Robey. Dynamics of CD8 T cell priming by dendritic cells in intact lymph nodes. *Nature Immunology*, 4:579–585, 2003.
- [10] Susanna Celli, Mark Day, Andreas J Müller, Carmen Molina-Paris, Grant Lythe, and Philippe Bousso. How many dendritic cells are required to initiate a T-cell response? *Blood*, 120(19):3945–3948, 2012.
- [11] Jun Abe, Shigeeyuki Shichino, Satoshi Ueha, Shin-ichi Hashimoto, Michio Tomura, Yutaka Inagaki, Jens V Stein, and Kouji Matsushima. Lymph node stromal cells negatively regulate antigen-specific CD4⁺ T cell responses. *Journal of Immunology*, 193(4):1636–1644, 2014.
- [12] A. Link, T.K. Vogt, S. Favre, M.R. Britschgi, H. Acha-Orbea, B. Hinz, J.G. Cyster, and S.A. Luther. Fibroblastic reticular cells in lymph nodes regulate the homeostasis of naive T cells. *Nature Immunology*, 8(11):1255–1265, 2007.
- [13] Ramon Roozendaal and Reina E Mebius. Stromal cell-immune cell interactions. *Annual Review of Immunology*, 29:23–43, 2011.
- [14] Omar Khan, Mark Headley, Audrey Gerard, Wei Wei, Limin Liu, and Matthew F Krummel. Regulation of T cell priming by lymphoid stroma. *PLoS ONE*, 6(11):e26138, 2011.
- [15] Lucas Onder, Priyanka Narang, Elke Scandella, Qian Chai, Maria Iolyeva, Kerim Hoorweg, Cornelia Halin, Ellen Richie, Paul Kaye, Jürgen Westermann, Tom Cupedo, Mark Coles, and Burkhard Ludewig. IL-7-producing stromal cells are critical for lymph node remodeling. *Blood*, 120(24):4675–4683, 2012.
- [16] Thea Hogan, Andrey Shuvaev, Daniel Commenges, Andrew Yates, Robin Callard, Rodolphe Thiébaud, and Benedict Seddon. Clonally diverse T cell homeostasis is maintained by a common program of cell-cycle control. *Journal of Immunology*, 190(8):3985–3993, 2013.
- [17] Jung-Hyun Park, Qing Yu, Batu Erman, Jacob S Appelbaum, Diego Montoya-Durango, H Leighton Grimes, and Alfred Singer. Suppression of IL7R α transcription by IL-7 and other prosurvival cytokines: a novel mechanism for maximizing IL-7-dependent T cell survival. *Immunity*, 21(2):289–302, 2004.
- [18] Megan J Palmer, Vinay S Mahajan, Jianzhu Chen, Darrell J Irvine, and Douglas A Lauffenburger. Signaling thresholds govern heterogeneity in IL-7-receptor-mediated responses of naïve CD8⁺ T cells. *Immunology and Cell Biology*, 89(5):581–594, 2011.
- [19] E.P. Kaldjian, J.E. Gretz, A.O. Anderson, Y. Shi, and S. Shaw. Spatial and molecular organization of lymph node T cell cortex: a labyrinthine cavity bounded by an epithelium-like monolayer of fibroblastic reticular cells anchored to basement membrane-like extracellular matrix. *International Immunology*, 13(10):1243, 2001.

- [20] S.N. Mueller and R. Ahmed. Lymphoid stroma in the initiation and control of immune responses. *Immunological Reviews*, 224(1):284–294, 2008.
- [21] Flavian D Brown and Shannon J Turley. Fibroblastic reticular cells: Organization and regulation of the T lymphocyte life cycle. *Journal of Immunology*, 194(4):1389–1394, 2015.
- [22] Alexey Kislitsyn, Rostislav Savinkov, Mario Novkovic, Lucas Onder, and Gennady Bocharov. Computational approach to 3d modeling of the lymph node geometry. *Computation*, 3(2):222–234, 2015.
- [23] M. Bajénoff, J.G. Egen, L.Y. Koo, J.P. Laugier, F. Brau, N. Glaichenhaus, and R.N. Germain. Stromal cell networks regulate lymphocyte entry, migration, and territoriality in lymph nodes. *Immunity*, 25(6):989–1001, 2006.
- [24] J.B. Beltman, A.F.M. Maree, J.N. Lynch, M.J. Miller, and R.J. de Boer. Lymph node topology dictates T cell migration behavior. *Journal of Experimental Medicine*, 204(4):771, 2007.
- [25] S.N. Mueller and R.N. Germain. Stromal cell contributions to the homeostasis and functionality of the immune system. *Nature Reviews Immunology*, 9:618–629, 2009.
- [26] M. Sixt, N. Kanazawa, M. Selg, T. Samson, G. Roos, D.P. Reinhardt, R. Pabst, M.B. Lutz, and L. Sorokin. The conduit system transports soluble antigens from the afferent lymph to resident dendritic cells in the T cell area of the lymph node. *Immunity*, 22(1):19–29, 2005.
- [27] Jason G Cyster. Chemokines and cell migration in secondary lymphoid organs. *Science*, 286(5447):2098–2102, 1999.
- [28] Michael E Meyer-Hermann and Philip K Maini. Interpreting two-photon imaging data of lymphocyte motility. *Physical Review E*, 71(6):061912, 2005.
- [29] Bernd H Zinselmeyer, John Dempster, Alison M Gurney, David Wokosin, Mark Miller, Hsiang Ho, Owain R Millington, Karen M Smith, Catherine M Rush, Ian Parker, Michael Cahalan, James M Brewer, and Paul Garside. In situ characterization of CD4⁺ T cell behavior in mucosal and systemic lymphoid tissues during the induction of oral priming and tolerance. *Journal of Experimental Medicine*, 201(11):1815–1823, 2005.
- [30] C. Beauchemin, N.M. Dixit, and A.S. Perelson. Characterizing T cell movement within lymph nodes in the absence of antigen. *Journal of Immunology*, 178(9):5505, 2007.
- [31] Johannes Textor, Sarah E Henrickson, Judith N Mandl, Ulrich H von Andrian, Jürgen Westermann, Rob J de Boer, and Joost B Beltman. Random migration and signal integration promote rapid and robust T cell recruitment. *PLoS Computational Biology*, 10(8):e1003752, 2014.
- [32] Henry P Mirsky, Mark J Miller, Jennifer J Linderman, and Denise E Kirschner. Systems biology approaches for understanding cellular mechanisms of immunity in lymph nodes during infection. *Journal of Theoretical Biology*, 287:160–170, 2011.
- [33] Zvi Grossman, Martin Meier-Schellersheim, Ana E Sousa, Rui MM Victorino, and William E Paul. CD4⁺ T-cell depletion in HIV infection: are we closer to understanding the cause? *Nature Medicine*, 8(4):319–323, 2002.
- [34] Andrew Yates, Jaroslav Stark, Nigel Klein, Rustom Antia, and Robin Callard. Understanding the slow depletion of memory CD4⁺ T cells in HIV infection. *PLoS Medicine*, 4(5):e177, 2007.
- [35] Changwang Zhang, Shi Zhou, Elisabetta Groppe, Pierre Pellegrino, Ian Williams, Persephone Borrow, Benjamin M Chain, and Clare Jolly. Hybrid spreading mechanisms and T cell activation shape the dynamics of HIV-1 infection. *PLoS Computational Biology*, 11(4):e1004179, 2015.

- [36] Saikrishna Gadhamsetty, Joost B Beltman, and Rob J de Boer. What do mathematical models tell us about killing rates during HIV-1 infection? *Immunology letters*, 168(1):1–6, 2015.
- [37] Timothy W Schacker, Cavan Reilly, Gregory J Beilman, Jodie Taylor, David Skarda, David Krason, Matthew Larson, and Ashley T Haase. Amount of lymphatic tissue fibrosis in HIV infection predicts magnitude of HAART-associated change in peripheral CD4 cell count. *AIDS*, 19(18):2169, 2005.
- [38] Ming Zeng, Peter J Southern, Cavan S Reilly, Greg J Beilman, Jeffrey G Chipman, Timothy W Schacker, and Ashley T Haase. Lymphoid tissue damage in HIV-1 infection depletes naive T cells and limits T cell reconstitution after antiretroviral therapy. *PLoS Pathogens*, 8(1):e1002437, 2012.
- [39] Ming Zeng, Mirko Paiardini, Jessica C Engram, Greg J Beilman, Jeffrey G Chipman, Timothy W Schacker, Guido Silvestri, and Ashley T Haase. Critical role of CD4 T cells in maintaining lymphoid tissue structure for immune cell homeostasis and reconstitution. *Blood*, 120(9):1856–1867, 2012.
- [40] Lintao Zhao, Lina Liu, Jianbao Gao, Yang Yang, Chunyan Hu, Bo Guo, and Bo Zhu. T lymphocytes maintain structure and function of fibroblastic reticular cells via lymphotoxin (LT)-B. *BMC Immunology*, 15(1):33, 2014.
- [41] Graham M Donovan and Grant Lythe. T-cell movement on the reticular network. *Journal of Theoretical Biology*, 295:59–67, 2012.
- [42] Alan S Perelson and Ruy M Ribeiro. Modeling the within-host dynamics of HIV infection. *BMC Biology*, 11(1):96, 2013.
- [43] Mélanie Prague, Daniel Commenges, and Rodolphe Thiébaud. Dynamical models of biomarkers and clinical progression for personalized medicine: The HIV context. *Advanced Drug Delivery Reviews*, 65(7):954–965, 2013.
- [44] Jennifer J Linderman, Thomas Riggs, Manjusha Pande, Mark Miller, Simeone Marino, and Denise E Kirschner. Characterizing the dynamics of CD4+ T cell priming within a lymph node. *Journal of Immunology*, 184(6):2873–2885, 2010.
- [45] Reuven Y Rubinstein and Dirk P Kroese. *Simulation and the Monte Carlo method*, volume 707. John Wiley and Sons, 2011.
- [46] Charles R Doering, Khachik V Sargsyan, and Leonard M Sander. Extinction times for birth-death processes: Exact results, continuum asymptotics, and the failure of the Fokker–Planck approximation. *Multiscale Modeling and Simulation*, 3(2):283–299, 2005.
- [47] Tuan Le, Edwina J Wright, Davey M Smith, Weijing He, Gabriel Catano, Jason F Okulicz, Jason A Young, Robert A Clark, Douglas D Richman, Susan J Little, et al. Enhanced CD4+ T-cell recovery with earlier HIV-1 antiretroviral therapy. *New England Journal of Medicine*, 368(3):218–230, 2013.
- [48] Marc Barthélemy. Spatial networks. *Physics Reports*, 499(1):1–101, 2011.
- [49] Johannes Textor, Mathieu Sinn, and Rob J de Boer. Analytical results on the Beauchemin model of lymphocyte migration. *BMC Bioinformatics*, 14(Suppl 6):S10, 2013.
- [50] Z Schuss, A Singer, and David Holcman. The narrow escape problem for diffusion in cellular microdomains. *Proceedings of the National Academy of Sciences*, 104(41):16098–16103, 2007.

A Properties of the model

Construction of the network

We follow the approach of [41] by first explicitly constructing the RN network, and then confining all cell motion to it. Our spatial random networks [48] are constructed by first positioning vertices at random, by sampling from the uniform distribution, and then generating edges between them. The position of each of the N vertices is independently drawn from the uniform distribution inside a sphere of radius R . Cells travel at a constant speed, changing direction upon reaching a vertex, where a T cell selects a new edge at random. This type of motion on a network may be approximated, after many turns, by a Brownian motion in three space dimensions whose diffusivity depends on the probability density of edge lengths, l [41, 49]:

$$D = \frac{v \mathbb{E}(l^2)}{6 \mathbb{E}(l)}. \quad (11)$$

Subsets of the network are marked as exits and entrances *a priori*: in a LN which a sphere of radius R , vertices have coordinates (x, y, z) in cartesian coordinates, or radius r in spherical coordinates. Then exit edges are those with $r > 0.9R$ and $z > 0$ for both vertices, while entrances are vertices with $z < -0.75R$.

Transit times

Given the geometry of our model, a key measure is the transit time – the time taken by a cell between entering the network, and leaving again. The mean time for a Brownian motion with diffusivity D is

$$\tau_D = \frac{\pi R^3}{3aD} \quad (12)$$

where a the radius of the exit on the surface of the sphere [50]. Using our effective diffusivity estimate for network motion [41], we find that

$$\tau \propto \frac{R^2 N^{1/3}}{av}, \quad (13)$$

where N is the number of vertices and v the constant velocity parameter of motion. We find this scaling argument agrees well with the simulation results.

Parameters

The parameters used are given in Table 1. For $R = 150 \mu\text{m}$ and $V = 1000$, we find $\bar{T}_0 \sim 1800$ from direct fitting. For $R = 300 \mu\text{m}$, and $V = 5000$, we obtain $\tau = 0.98 \pm 0.02$ days with mean edge length $22.7 \mu\text{m}$.

B The steady state of the heterogeneous population model

Here we find the solution of the equations

$$\alpha \frac{dC}{dx} = -C(x) + \beta C(2x) \quad x \geq X \quad (14a)$$

$$\bar{x} \frac{dC}{dx} = -C(x) + 4 \frac{\lambda}{\mu} C(2x) \quad X/2 < x < X, \quad (14b)$$

where

$$\alpha = \frac{\bar{x}}{1 + \frac{\lambda}{\mu}} \quad \text{and} \quad \beta = \frac{4\lambda}{\mu + \lambda}.$$

μ	T cell death rate	$1/365 \text{ day}^{-1}$
μ_{HIV}	increased T cell death rate in HIV	$5.4 \times 10^{-3} \text{ day}^{-1}$
λ	T cell division rate (IL-7 dependent)	$10/365 \text{ day}^{-1}$
X	IL-7 division threshold	10 a.u.
ρ	rate of traffic from periphery to LN	2 day^{-1}
γ	deposition of LT- β onto network from trafficking T cells	$3/365 \text{ a.u. day}^{-1}$
$\tilde{\nu}$	IL-7 production rate	$15/365 \text{ a.u. day}^{-1}$
V	number of vertices in RN	5000
	FRC length	10 μm
β	FRC consumption rate of LT- β	$1/365 \text{ a.u. day}^{-1}$
R	radius of LN	300 μm
κ	collagenation rate in HIV	$3.8 \times 10^{-4} / \text{day}$

Table 1: Parameter values, determined from experimental data where available. The HIV-active rates μ_{HIV} and κ are fitted to the data of [47]. The FRC length is chosen to align with experimental data, e.g. [22]. The number of vertices, and radius of the LN, are chosen as large as possible within constraints of computational complexity for the agent-based model, while both maintaining a reasonable edge length [41]. Other parameters values were chosen phenomenologically.

If, for $x \geq X$, we write

$$C(x) = c_0 e^{-x/\alpha} + c_1 e^{-2x/\alpha} + c_2 e^{-4x/\alpha} + \dots,$$

then (14a) is satisfied if

$$c_i = -\frac{\beta}{2^i - 1} c_{i-1}, \quad i \geq 1.$$

Using (1), we require $\int_X^\infty C(x) dx = \frac{\mu}{\lambda}$ or

$$\alpha c_0 \left(e^{-X/\alpha} - \beta e^{-2X/\alpha} + \frac{1}{3} \beta^2 e^{-4X/\alpha} + \dots \right) = \frac{\mu}{\lambda}. \quad (15)$$

Now the task is to solve (14b). The solution of the differential equation

$$\frac{d}{dx} C_i(x) + \frac{1}{x} C_i(x) = A \exp\left(-k_i \frac{x}{\bar{x}}\right),$$

with $C_i(X/2) = 0$ is

$$C_i(x) = \frac{\bar{x} A}{k_i - 1} \left(\exp\left(-\frac{1}{2}(k_i - 1) \frac{X}{\bar{x}} - \frac{x}{\bar{x}}\right) - \exp\left(-k_i \frac{x}{\bar{x}}\right) \right).$$

The solution of (14b) is thus

$$C(x) = 4 \frac{\lambda}{\mu} \sum_{i=0}^{\infty} \frac{c_i}{k_i - 1} \left(\exp\left(-\frac{1}{2}(k_i - 1) \frac{X}{\bar{x}} - \frac{x}{\bar{x}}\right) - \exp\left(-k_i \frac{x}{\bar{x}}\right) \right), \quad (16)$$

where $k_i = 2^{i+1}(1 + \frac{\lambda}{\mu})$. The two conditions, (15) and continuity of $C(x)$ at $x = X$, allow us to find the two unknowns, \bar{x} and c_0 . In Figure 8, we compare the steady-state values of the mean number of cells, \bar{n} , and the mean IL-7 level, \bar{x} , obtained from numerical solution of the heterogeneous population model introduced in Section 3, with the following approximation, obtained using only the first term in (15) and (16):

$$\bar{x} \simeq \frac{X}{2} \left(\log \frac{4\lambda}{\mu + 2\lambda} \right)^{-1}.$$

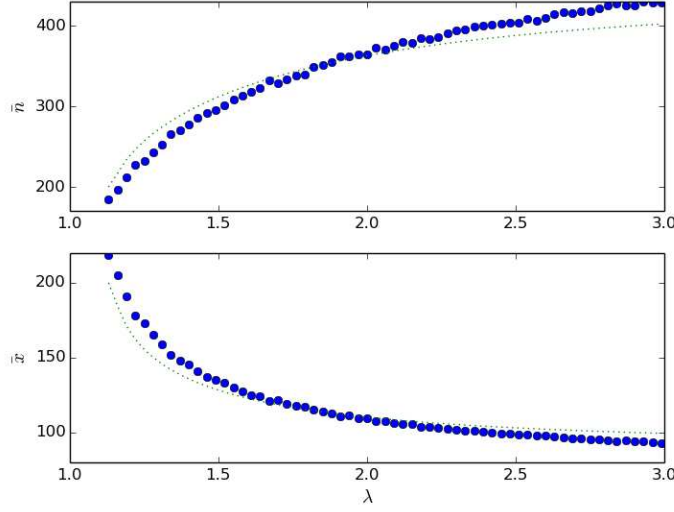


Figure 8: Mean total number of cells, and mean IL-7 level per cell versus λ , for the heterogeneous population model. Numerical results are compared with the formulae of this appendix. $\mu = 1.0$, $X = 10^2$, $\nu = 4 \times 10^4$.

C Derivation of the ODE model

Here we give the derivation of the ODE model, (6a)–(6d), from the PDE model, (5a)–(5c). We first neglect F and consider T and P integrated with respect to I . We split the integrals at the division threshold so that

$$\bar{T} = \int_0^\infty T dI = \underbrace{\int_0^X T dI}_{=\tilde{T}} + \underbrace{\int_X^\infty T dI}_{=\tilde{T}^*} \quad (17)$$

and similarly for P . Then by integration we obtain

$$\frac{d\tilde{P}}{dt} = -(\mu + \rho)\tilde{P} + c_o\tilde{T} + 2\lambda \int_X^{2X} P(I, t) dt \quad (18a)$$

$$\frac{d\tilde{P}^*}{dt} = -(\mu + \rho)\tilde{P}^* + c_o\tilde{T}^* - \lambda\tilde{P}^* + 2\lambda \int_{2X}^\infty P(I, t) dt \quad (18b)$$

$$\frac{d\tilde{T}}{dt} = -(\mu + c_o)\tilde{T} + \rho\tilde{P} - \left[\frac{\tilde{\nu}\bar{F}g(\tilde{T})}{\tilde{T}} T \right] \Big|_{I=X} \quad (18c)$$

$$\frac{d\tilde{T}^*}{dt} = -(\mu + c_o)\tilde{T}^* + \rho\tilde{P}^* + \left[\frac{\tilde{\nu}\bar{F}g(\tilde{T})}{\tilde{T}} T \right] \Big|_{I=X}. \quad (18d)$$

If we make the approximations

$$\begin{aligned} \int_X^{2X} P(I, t) dt &\approx \tilde{P}^* \\ \int_{2X}^\infty P(I, t) dt &\approx 0 \end{aligned}$$

(that is, that the P distribution above the level $2X$ is negligible) and that

$$\frac{T|_{I=X}}{\bar{T}} \propto k\tilde{T} \quad (19)$$

and variation in $g(\bar{T})$ is negligible near equilibrium, then assuming \bar{F} is constant, taking the constant f to approximate $\left[\frac{\bar{F}g(\bar{T})}{T}T\right]_{I=X}$ and dropping the tildes we obtain (6a)–(6d).